Journal of Heat and Mass Transfer Research

Journal homepage: https://jhmtr.semnan.ac.ir

Semnan University

ISSN: 2383-3068

Research Article

Artificial Neural Network Approaches for Predicting the Heat Transfer in a Mini-Channel Heatsink with Alumina/Water Nanofluid

Mohammad Mahdi Tafarroj [a]*, Seyed Soheil Mousavi Ajarostaghi [b], C.J. Ho [c], Wei-Mon Yan [d,e]*

[a] *Mechanical Engineering Department, Faculty of Engineering, Lorestan University, P.O. Box 68151-44316, Khorramabad, Iran*

[b] *Mechanical Engineering Department, Université de Sherbrooke, Sherbrooke, QC J1K 2R1, Canada*

[c] *Department of Mechanical Engineering, National Cheng-Kung University, Tainan 70101, Taiwan*

[d] *Department of Energy and Refrigerating Air-Conditioning Engineering, National Taipei University of Technology, Taipei 10608, Taiwan*

[e] *Research Center of Energy Conservation for New Generation of Residential, Commercial, and Industrial Sectors, National Taipei, University of Technology, Taipei 10608, Taiwan*

ARTICLE INFO

Article history:

Received: 2024-02-07

Revised: 2024-03-15

Accepted: 2024-03-16

Keywords:

Artificial Neural Network (ANN);

Mini-Channel heatsink;

Multilayer perceptron;

Radial basis function;

Simulated annealing.

ABSTRACT

This work uses artificial neural networks to evaluate heat transfer in a mini-channel heatsink using an alumina/water nanofluid. The multi-layer perceptron (MLP) and radial basis function (RBF) neural networks are employed for the modeling. To apply the artificial neural network analysis, 60 data of experimental works are utilized. The outcomes depicted that the simulated annealing (SA) technique significantly increased the performance of the RBF network, although the optimal MLP structure was discovered by trial and error. The optimized RBF network carried over more data with less than 2% errors as compared to the MLP. While the results of the MLP network showed that the average relative error for the test data set was 2.0496%, this value was 1.417% for the RBF network. The modeling time is a significant determining element when choosing the optimal technique. The RBF network optimization took longer than 60 minutes, even though all MLP structures were run 100 times in less than 15 minutes. In summary, artificial neural networks are effective instruments for simulating these kinds of processes, and their application can save a lot of time-consuming experimentation. Additionally, the RBF network outperforms the MLP in terms of precision while requiring less processing time.

1. Introduction

Due to the development of microelectronics, the cooling of electronic devices has an important effect on their performance and life by drastically increasing the density of chips and current voltage handling capability, which would cause high heat accumulation in the electronic devices. Minichannel (or microchannel) heat sinks are the best tools to improve high heat accumulation because of their higher heat transfer performance, smaller geometric size and volume per heat load, lower coolant requirement, lower operational cost, etc. Yet, the thermal efficiency of a minichannel heat sink is limited because of the

* **Corresponding author.**
E-mail address: *tafarroj.mm@lu.ac.ir and wmyan@ntut.edu.tw*

Cite this article as:
Tafarroj, M.M., Mousavi Ajarostaghi, S.S., Ho, C.J., Yan, W., 2024. Artificial Neural Network Approaches for Predicting the Heat Transfer in a Mini-Channel Heatsink with Alumina/Water Nanofluid. *Journal of Heat and Mass Transfer Research*, 11(1), pp. 75-88.
https://doi.org/10.22075/JHMTR.2024.32947.1520

thermal conductivity and specific heat of the coolants [1].

Hadi et al. [2] examined the effects of superhydrophobic coatings on the heat transfer and pressure drop in integral mini-channel heat sinks using distilled water and TiO_2 nanofluids at concentrations of 0.01% and 0.02%. Testing at power inputs of 40, 55, and 70 watts and varying volumetric flow rates, the research finds significant improvements in heat transfer and notable reductions in pressure drop across different mediums. The superior performance of the superhydrophobic-coated mini-channel heat sinks, validated against theoretical models, demonstrates their potential for enhanced thermal management in various applications, outperforming standard mini-channel heat sinks.

In the experimental work of Ho et al. [3], the heat dissipation of a parallel mini-channel heat sink with a latent heat cooling ceiling was evaluated. Utilizing alumina/water nanofluid with varied nanoparticle concentrations, the study assesses the impact of several parameters, including nanoparticle mass fraction, Reynolds number, and temperatures of the bottom wall, fluid inlet, and cooling plate, on the system's efficiency. Results showed that the nanofluid inlet temperature marginally affects friction factor at specific Reynolds numbers and significantly impacts it at others. Ghasemi et al. [4] conducted experimental research to assess the effectiveness of Al_2O_3 (alumina) nanoparticles in a circular minichannel heat sink for cooling electronic components like CPUs. The experiments varied the channels' hydraulic diameter and the coolant's flow rates. Data analysis proved that reducing the channel diameter and increasing the flow rate of the Al_2O_3-water nanofluid significantly enhances the cooling performance of the heat sinks. To address the complex interplay of channel size, nanofluid flow rates, and the number of channels on pressure drop and heat transfer, an optimization study was carried out using Response Surface Methodology (RSM) based on Central Composite Design (CCD).

Khan et al. [5] analyzed the cooling performance of straight, wavy, and dual-wavy micro-channel heat exchangers using ANSYS Fluent. Alumina-based nanofluids with concentrations of 1%, 3%, and 6% were used in a laminar flow regime. The investigation focused on parameters like Nusselt number, pressure drop, base temperature, and Thermal Performance Factor (TPF) across a Reynolds number range of 100–900. Results showed that wavy and dual wavy channels enhance convective heat transfer more effectively than straight channels, attributed to secondary vortices formation in curved sections. In the other research, Dastafkan et al. [6] explored the effects of alumina nanoparticles and channel waviness on the heat transfer and pressure drop in a minichannel, focusing on comparing straight and wavy channels.

In the work of Topcu et al. [7], a computer model of the Zalman ZM-WB_3 Gold heat exchanger, a liquid-cooled computer processor, was validated against existing models and experimental data. The research explored variations in fin thickness, fin height, and cooling fluid types using Ansys Fluent 17.1 for Computational Fluid Dynamics analysis. Different configurations were tested, including various fin dimensions and cooling fluids. The study concluded that a CPU's most effective cooling performance is achieved using a CuO-H_2O nanofluid with a 2.25% volume ratio in a heat exchanger with 5.5 mm fin height and 2.0 mm fin thickness.

Saghafian et al. [8] numerically investigated the hydrodynamic and heat transfer characteristics of electroosmotic flow in a microfluidic system influenced by lateral electric and transverse magnetic fields. Hameed and Saha [9] focused on the thermo-hydraulic analysis of oil-MWCNT nano-fluid flow in rectangular channels with embedded obstacles under uniform heat flux, investigated numerically using the finite volume approach and Fluent software. The research examined how the shape of obstacles, nanoparticle volume fraction, and Reynolds number affect the flow phenomena. Ramesh et al. [10] reviewed the flow of Carreau nanofluids in micro-channels within the context of microfluidic technology and Micro Electromechanical Systems (MEMS), focusing on effects like electro-osmosis, Joule heating, chemical reactions, and the impact of external magnetic fields. Utilizing the regular perturbation method and a Cartesian coordinate system, their study presented graphical analyses of fluid flow characteristics such as velocity, temperature, solutal nano-particle concentration, and Sherwood and Nusselt numbers under varying conditions.

A numerical analysis was done to enhance a mini-channel heat sink's heat transfer coefficient [11]. A new shape for mini-channels was proposed to compare with the rectangular channels using pure water and (Fe_3O_4 and Ag-water) nanofluids as coolants. The base temperature, friction factor, Nusselt Number, and thermal resistance have been studied. The minichannel heatsink is exposed with a constant heat flux (180 kW/m^2) at the bottom. The results showed that nanofluid and (converge-diverge) mini-channel can enhance the heat sink's hydrothermal performance, and (Ag-H_2O) nanofluid has superior heat transfer performance compared to the Fe_3O_4 nanofluid. Lan et al. [12]

have designed a minichannel heat sink (MCHS) with twisted tape inducing swirling flow. The cross-section of the minichannel was square, and the width, height and length of the minichannel were respectively 2 mm, 2 mm and 150 mm. The flow boiling heat transfer and instability in MCHS were experimentally inspected under two mass fluxes, two inlet temperatures, and a range of heat flux. Results demonstrated that the swirling flow can reduce the rapid growth of bubbles and, suppress the coalescence of small bubbles effectively, and also cause the bubbles to produce helical motion behavior. A new type of air-cooled heat sink was designed by Nemati et al. [13]. It consists of several layers of minichannels. In the design, the hydraulic diameter was smaller than in conventional heat sinks, and therefore, the achievable heat transfer rates were higher. The performance of the designed heat sink was compared to a plate-fin heat sink. The comparison shows that entropy generation in the latter is about 27% higher than in the former.

Computational Intelligence (CI) methods, including Fuzzy Logic (FL), Genetic Algorithm (GA), and Artificial Neural Networks (ANNs), have been used effectively in many scientific research and engineering projects. The ANNs have been developing for about three decades and are now extensively employed in many applications, especially thermal systems. ANNs propose a new approach to model nonlinear, uncertain complex systems without explicit knowledge of input/output relationships. It can be used to learn complex nonlinear relationships from a set of related input/output vectors. It enables dynamic simulation and control of unknown or uncertain processes.

Recently, ANNs have been utilized in various thermal systems to investigate heat transfer characteristics, performance estimation, and dynamic control. Esfe [14] modeled the heat transfer process and fluid flow of a water-based nanofluid with Ag nanoparticle with volume fractions below 1% in a heat exchanger by ANN with radial basis transfer function (RBFNN). The modeling has been done by postprocessing the experimental results. The modeled control parameters were relative to the pressure loss and the Nusselt number, in which the related data regression coefficients were achieved by 99.54 and 99.76%, respectively.

Longo et al. [15] presented an ANN model to study refrigerant condensation in herringbone-type Brazed Plate Heat Exchangers. The inputs are the geometrical and operational parameters as well as refrigerant properties. The results used included 1884 data points obtained from 12 plate geometries and 16 refrigerants. The presented ANN model reported a Mean Absolute Percentage Error of 3.6%. In the other work, the ANN model has been developed to predict the Cu/CNTs-water hybrid nanofluids flow and heat transfer in a U-shaped heat exchanger by Maddah et al. [16]. Various volume concentrations of considered hybrid nanofluids and inlet temperatures have been analyzed. The ANN model has been used to calculate the exergy efficiency in the proposed heat exchanger and under-considered operational conditions. Accordingly, a three-layer model with seven neurons in the hidden layer with a precision of $R_2 = 0.9967$ has been presented, indicating that the presented ANN model tracks a normal distribution. Moya-Rico et al. [17] used an ANN model to predict the heat transfer and pressure loss in a triple pipe heat exchanger containing non-corrugated and corrugated pipes (nine different types with various pitches and depths). The prediction has been performed based on the 181 experimental results. The considered working fluid is commonly used in the food industry. The results showed that the ANN model presented a mean relative error below 4% compared to the experimental results. Shojaeefard et al. [18] considered an air-to-refrigerant laminated-type evaporator and presented a novel ANN model to predict heat transfer and fluid flow parameters. The studied evaporator considered and analysed both single- and two-phase conditions. The results showed that inlet refrigerant pressure was the most important factor in calculating the evaporator capacity.

Also, besides the above literature review, the ANN model has been used to predict the efficient parameters of heat transfer in the minichannels and heat sinks. Uysal and Korkmaz [19] presented an ANN model based on the obtained numerical results of investigating heat transfer of water/Ag-MgO hybrid nanofluid in a rectangular minichannel. The Reynolds number and volume concentration considered are 200-2000 and 0.005-0.02, respectively. The ANN method could create a model to calculate the entropy generation in the proposed thermal system. Results depicted that total entropy generation augments by raising the proposed nanoparticle volume fraction. Tafarroj et al. [20] presented an ANN model to calculate the amount of heat transfer of water/TiO_2 nanofluid flow in a microchannel heat sink, which includes 40 channels with dimensions of 4cm×500μm×800μm. The datasets have been collected with three thermal conductivity, two Reynolds numbers, three heating rates, and four volume concentrations. The network output was the Nusselt number. Results presented that average relative errors of heat transfer coefficients and Nusselt number were 0.2 and 0.3%, respectively. By performing experimental tests, Motahar and Jahangiri [21] focused on a

phase change material (PCM) heat sink. The ANN model was used to evaluate the heat transfer coefficient. Results showed that usage of PCM decreases the transient temperature. Also, the presented ANN calculates the transient Nusselt number with great precision. Salehfekr Arabani et al. [22] introduced an ANN model to predict the first-law and second-law efficiencies in an innovative helical heat sink. The working fluid was water/Ag nanofluid. The numerical simulations have been done for various geometrical parameters of the proposed heat sink, Re numbers, and nanofluid volume concentrations. Results indicated that the maximum first-law belongs to the case with *Re*=1500 and a concentration of 1%. The ANN model was used based on numerical datasets to predict entropy generation (thermal and frictional types).

Zheng et al. [23] employed machine learning in the heat exchange channels. The performance of various ML techniques was compared to predict the heat transfer coefficient. In the subject of heat transfer, neuron-based methods are more suitable. Sensitivity analysis and ML together portend a promising future. Genetic algorithms were utilized with ML to enhance structural optimization. Liu and Liu [24] used the ML model to lower the experimental uncertainty and analyze better the ammonia engine performance. They fitted a spark plug to the original compression ignition engine to regulate and start the ammonia combustion process. According to the results, the random forest approach had border underfitting, while the gradient-boosting regression trees algorithm had overfitting issues. Furthermore, the artificial neural network technique outperformed support vector regression's ability to identify the correlation between engine control factors and ammonia engine performance.

The present study employs ANNs to investigate the heat transfer rate in a mini-channel heat sink. Limited measured results were employed to train and test ANN configurations. The error back-propagation (EBP) algorithm trains and tests the network. Predictions of the average Nusselt number were made. Different network configurations are also investigated by searching for relatively better networks to make predictions.

2. Experimental Study and Data Reduction

Heat exchangers are essential to many sectors because they improve energy efficiency, streamline operations, and have a more minor environmental impact. They lower operating costs and energy consumption by enabling the recovery and reuse of waste heat and promoting heat transfer across fluids without mixing them [25]. Heat exchangers also play a critical role in preserving the exact temperature conditions needed for product quality and yield, helping to create safer manufacturing settings by avoiding overheating and dangerous situations [26]. Because of their efficiency and versatility, they are essential to many different industries, including chemical processing, power generation, oil and gas, pharmaceuticals, food and beverage, and power production. This highlights their importance in contemporary industrial processes [27].

Some experimental works [28–33] were presented to study the impact of utilizing water-based nanofluids, including Al_2O_3 particles. The experimental setup is schematically depicted in Fig. 1. The working fluid entered the system from a tank through a filter by a centrifugal pump. Two constant temperature bathes were employed to set the inlet and outlet fluid temperatures at specific values. Eight rectangular mini-channel heatsinks of copper with dimensions 1×1.5×50 mm are considered. Two temperature sensors were used, including resistance temperature detectors (RTDs) and T-type thermocouples with two and seven numbers, respectively. These T-type thermocouples spaced equidistantly at a thickness of 3 mm beneath the minichannel base surface across the heat sink base centerline were used to determine the local wall temperatures. The volumetric flow rate was adjusted using a flow meter. The constructed test module comprised a minichannel heat sink, two plate heaters, a cover plate, and housing. The inlet and outflow pendulums were made to ensure homogenous flow distribution. With a fin width of 1 mm, ten parallel, rectangular minichannels were machined at equal intervals. The minichannel has a 50 mm length, 1 mm width, and 1.5 mm height in its cross-section. The range of the considered Reynolds number is Re = 100-1500. A heater powered by a DC power supply provides the constant heat flux for the test section. Experimental tests for specific conditions usually got a steady state for about 1 hour. The data acquisition system records all measurement data. The related works entirely explained the provision of water-based nanofluids of Al_2O_3 particles [28–33].

During the experimental tests, the corrected electric power, $q_{o,corr}$, in the proposed heat sink was calculated by comparing the electric input power, q_o, in the steady-state heat transfer rate removed by the heat absorbed by the pure water flowing into the heatsink as:

$$q_{o,corr} \approx q_0 - \rho \dot{Q} c_p \left(T_{out} - T_{in} \right) \quad (1)$$

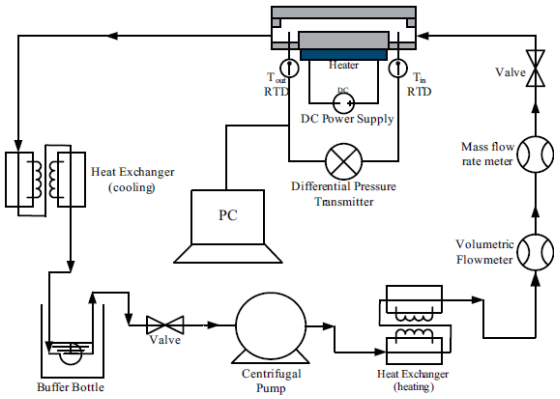

Fig. 1. Diagram of experimental facility [28–33]

The T_w, as centerline wall temperature, is calculated using the measured wall temperatures, T_{tc}, at different positions of the mini-channels. Assuming 1D thermal conduction among the planes of the thermocouple and mini-channel, the wall temperature is estimated as follows:

$$T_w = T_{tc} - \frac{q_{o,eff} t_c}{k_s A_{base}} \quad (2)$$

where $q_{o,eff}$ indicates the effective heat input absorbed by the working fluid.

The total base area of the heat sink is calculated as follows:

$$A_{base} = N(W_{ch} + W_{rib})L_{ch} \quad (3)$$

where N indicates the number of channels.

The heat transfer coefficient and average Nusselt number are calculated as follows:

$$\bar{h} = \frac{q_f}{(\bar{T}_w - T_{in})A_{base}} \quad (4)$$

$$\overline{Nu} = \frac{\bar{h}_{itd} D_h}{k} \quad (5)$$

3. Modeling Approaches

3.1. The Artificial Neural Networks

Various neural network structures are extensively introduced in the literature [34]. The feedforward neural networks are those allowing signal flows only in one direction. In addition, most of the feedforward neural networks are planned in some layers [35]. Bellow, two well-known feedforward types of these networks, the multilayer perceptron (MLP) and the radial basis function (RBF) neural networks [36], are introduced, and then, using these networks, the process is modeled [37]. Finally, the ability of the networks to model the process is compared.

3.1.1. The Concept of MLP Networks

In MLP networks, a layered architecture of neurons is designed. The information is passed through the layers, and the network will learn to fit its outputs to its target values. A simple representation of a network with three layers (two hidden layers and one output layer) has been demonstrated in Fig. 2. These types of neural networks are the most popular ones. Therefore, the MLP's procedure can be found in Ref. [38].

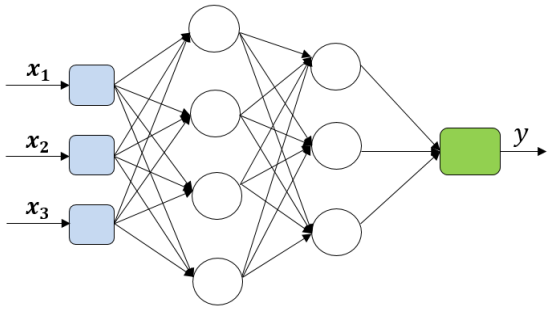

Fig. 2. A typical MLP neural network with three layers

3.1.2. Radial Basis Function Networks Architecture

The central concept of the RBF neural network is based on approximating an unknown function using linear combinations of non-linear functions named basis functions. The basis functions are radially symmetric about a center. An RBF neural network comprises three layers: an input layer, a single layer of non-linear processing neurons, and an output layer. The construction of a usual network for the output prediction is shown in Fig. 3.

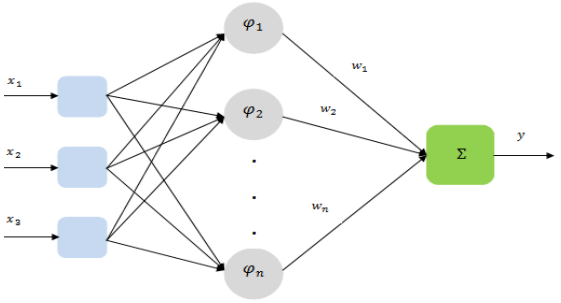

Fig. 3. The schematic representation of an RBF network

The network predicts the average Nusselt number ($\overline{Nu}$) as the output for a given set of inputs including solid volume fraction of nanoparticles (ω), heat flux, and Reynolds number (Re) of inlet fluid flow. The output of the RBF neural network is calculated via Eq. (6).

$$y = \sum_{k=1}^{n} w_k \varphi_k(\|\boldsymbol{x} - \boldsymbol{c_k}\|_2) \quad (6)$$

in Eq. (6), $\boldsymbol{x}$ is the input vector, φ_k is the processing function for the node number k of the hidden layer, $\|.\|_2$ is the Euclidean norm, w_k is the weight corresponding to the kth node of the hidden layer, n is the number of neurons in the hidden layer, and finally, $\boldsymbol{c_k}$ is the center of the basis function associated with the kth node in the input space. In each neuron, the Euclidean distance between the input and the corresponding center of the neuron is evaluated. Then, the output of the neuron is computed via a nonlinear function. At last, all neurons' outputs are weighted and summed, and network output is determined. In this work, the Gaussian transfer function has been selected as the radial basis function represented via Eq. (7).

$$\varphi(x) = e^{\frac{-x^2}{\sigma^2}} \tag{7}$$

in Eq. (7), the parameter σ is called the spread, and it controls the generality of the network performance. As seen in Eq. (6), two classes of parameters should be adjusted using the RBF networks: the weights, w_k and the centers, $\boldsymbol{c}_k$.

In this work, the new RBF in MATLAB software has been used for modeling. Constructing a powerful RBF model using the MATLAB toolbox must accurately tune two main network parameters. These parameters are the spread (σ) and the maximum number of neurons. So, a proper optimization algorithm can be helpful to find the best combination of these parameters. The simulated annealing algorithm (SA) is introduced in the next section.

3.2. Simulated Annealing Algorithm

Simulated annealing (SA) is one of the most potent yet easy-to-implement optimization algorithms. This algorithm was proposed by Kirkpatrick et al. [39]. Here, the pseudocode of the SA algorithm for minimizing an objective function *f(x)* can be expressed as [35]:

- Select an initial for the input variable x_0 randomly.
- Select a new point x in the neighborhood of the x_0
- Let $\Delta f = f(x) - f(x_0)$ and $p = \frac{-\Delta f}{T}$
- If $\Delta f < 0$, set $x_0 = x$ and go to 5; otherwise, generate a random value $\rho \in (0.1)$; if $\rho < p$, set $x_0 = x$ and go to 5, else go to 2.
- Reduce T by a linear or logarithmic formula (for example, $T = nT$ where 0 < n < 1)
- If the stopping criterion is unmet, go to 2 as the next iteration; otherwise, go to 7.
- Stop and report the optimal solution.
- As stated previously, this algorithm has been employed in the next section to set up the best possible RBF network.

4. Results and Discussion

This section discusses the results predicted by the introduced approaches (the MLP and the RBF networks). In the first subsection, the performance of the MLP network in predicting the problem outputs will be examined. Then, in the next part, the capability of the RBF network to model the problem will be evaluated. Finally, the results of the two networks will be compared, and a more proper network will be introduced.

The data used in the modeling process are shown in Table 1. As can be seen, the problem has three inputs and one output. To fairly judge the results of the two networks, the number of data used in training and testing procedures is equal in modelling with both models.

Before beginning analyses, it is helpful to check whether there is any outlier in the data set. If there are outliers, they should be removed from the data. A box plot of all data can help to find any possible outlier. The box plot of data has been plotted in Fig. 4.

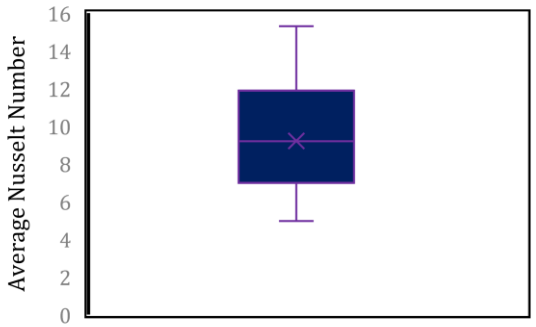

Fig. 4. The box plot of all data

According to Fig. 4, it can be observed that there is no outlier in the data set. Thus, all data can be implemented for building models.

4.1. The MLP model

One of the main challenges in MLP modeling is determining the best network structure to yield the best results. Generally, the MLP has some inputs, some hidden layers, and one output layer. The problem imposes the number of inputs and outputs. However, the main challenge arises when the number of hidden layers and the number of neurons in each hidden layer should be determined. In this case, it is common to use a trial-and-error procedure to find the best structure [26-28].

For modeling by the MLP technique, the data set should be divided into three subsets: the training set, the validating set, and the testing set. The training procedure is performed in the first step of the neural network using training and validating datasets. So, validation is a part of

training that guarantees the generality of the network performance [28]. Lastly, the test data will examine the network's ability, which are new to the network and have not been used in the training procedure. To better decide on the network's accuracy and precision, the network with a specific configuration was run 20 times. In each run, the data implemented in training, validating, and testing procedures are randomly picked up from all data.

Table 1. The data used in the modeling process

No.	Solid Volume Fraction of Nanoparticles (ω)	Heat Flux (w/m^2)	Reynolds Number (Re)	Average Nusselt Number ($\overline{Nu}$)	No.	Solid Volume Fraction of Nanoparticles (ω)	Heat Flux (w/m^2)	Reynolds Number (Re)	Average Nusselt Number ($\overline{Nu}$)
1	0	32000	239	4.971	31	0.05	32000	239	5.425
2	0	32000	420	7.201	32	0.05	32000	420	7.94
3	0	32000	689	8.22	33	0.05	32000	689	9.582
4	0	32000	962	9.885	34	0.05	32000	962	12.072
5	0	32000	1368	11.368	35	0.05	32000	1368	14.302
6	0	40000	242	5.193	36	0.05	40000	242	5.238
7	0	40000	423	6.892	37	0.05	40000	423	6.99
8	0	40000	693	8.647	38	0.05	40000	693	9.549
9	0	40000	963	9.985	39	0.05	40000	963	11.604
10	0	40000	1369	12.236	40	0.05	40000	1369	14.119
11	0	48000	245	5.446	41	0.05	48000	245	5.405
12	0	48000	426	7.457	42	0.05	48000	426	7.193
13	0	48000	698	8.897	43	0.05	48000	698	9.488
14	0	48000	970	10.457	44	0.05	48000	970	11.214
15	0	48000	1375	12.12	45	0.05	48000	1375	13.115
16	0.02	32000	239	5.032	46	0.1	32000	239	5.643
17	0.02	32000	420	7.153	47	0.1	32000	420	7.993
18	0.02	32000	689	8.448	48	0.1	32000	689	10.614
19	0.02	32000	962	10.077	49	0.1	32000	962	12.201
20	0.02	32000	1368	11.986	50	0.1	32000	1368	14.417
21	0.02	40000	242	5.123	51	0.1	40000	242	5.604
22	0.02	40000	423	6.504	52	0.1	40000	423	7.412
23	0.02	40000	693	8.641	53	0.1	40000	693	9.983
24	0.02	40000	963	10.011	54	0.1	40000	963	12.115
25	0.02	40000	1369	12.137	55	0.1	40000	1369	15.299
26	0.02	48000	245	5.421	56	0.1	48000	245	5.72
27	0.02	48000	426	6.991	57	0.1	48000	426	7.698
28	0.02	48000	698	8.85	58	0.1	48000	698	10.059
29	0.02	48000	970	10.632	59	0.1	48000	970	12.062
30	0.02	48000	1375	12.229	60	0.1	48000	1375	14.668

The performance of networks with different structures can be compared using some criteria. One of the most common criteria is the relative error RE determined by Eq. (8) for each test sample.

$$RE = \frac{t - y}{t} \times 100 \quad (8)$$

where y is the network prediction, and t is the target value. It should be noted that the sign of RE can determine the distribution of the errors around the zero value, which is the ideal value for the error. The absolute value of relative errors must be averaged for all test data to show the accuracy of the network prediction. So, the average relative error ($AvgRE$) is defined as Eq. (9).

$$AvgRE = \frac{\sum_{k=1}^{n} |RE_k|}{n} \quad (9)$$

where n is the number of test data. Another suitable way to check the network performance is the correlation coefficient between the predicted outputs and their targets. More details about the calculation of this coefficient can be found in Refs. [10, 33]. The last criterion is the standard deviation of the $AvgRE$ (i.e., $stdRE$), which indicates whether the prediction ability of the trained network is acceptable in multiple runs.

The number of all data is 60. Among all, 12 data are separated from the rest as the test data and 6 data are used to validate. Each network with a specific architecture was run 100 times. The results obtained from the MLP have been listed in Table 2. The table shows the network structure by the number of hidden layers, including neurons. For example, the structure {3} indicates that the network has one hidden layer with 3 neurons, and {3,7} shows that the network has two hidden layers with three neurons in the first hidden layer and seven neurons in the second hidden layer. Table 2 shows that generally, the networks with one hidden layer have better results. Considering all criteria simultaneously, it can be concluded that a network with one hidden layer and 11 neurons could be selected as the best one.

Table 2. The results of the MLP network calculated using the test data

Network Structure	*AvgRE*	*MinRE*	*stdRE*	*CorrCoef*
{3}	4.5300	1.9539	3.2966	0.9708
{7}	4.2500	1.2846	1.7951	0.9897
{11}	3.9455	2.0496	0.9388	0.9954
{15}	3.9364	2.1414	1.0325	0.9902
{19}	4.0551	2.4433	1.1020	0.9901
{23}	4.3047	1.9233	2.2375	0.9903
{3,3}	5.5231	1.9006	6.6050	0.9577
{3,7}	7.7874	1.7346	9.7504	0.9212
{3,11}	4.2080	2.2888	1.37	0.9890
{11,7}	5.5594	1.7140	7.1409	0.9125

The outputs of the best run are presented to visualize the results of the selected network. The predicted values against the targets for the train and test data sets have been illustrated in Fig. s 5 and 6. The absolute values of relative errors computed via Eq. (8) for the best run of the selected network have been demonstrated in Fig. 7. The maximum value of error is 5.59% according to data number 35 and the minimum one is 0.03% according to data number 50. Furthermore, 4 data have errors less than 1%, and 7 have relative errors less than 2%. Moreover, the average relative error for the test data set is 2.0496.

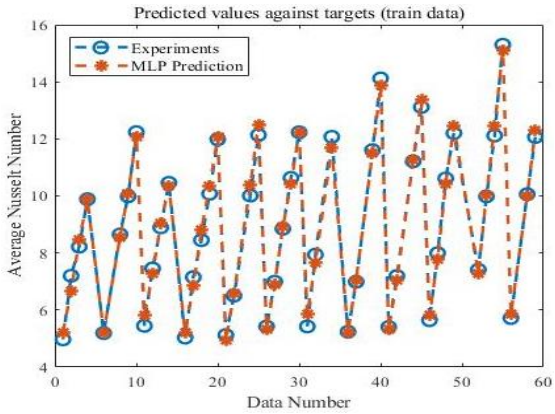

Fig. 5. The MLP performance based on the train data

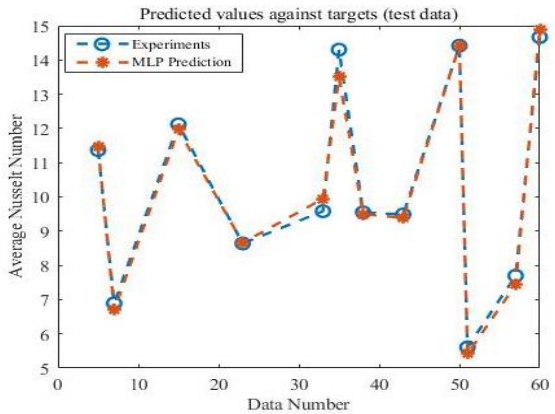

Fig. 6. The MLP performance based on the test data

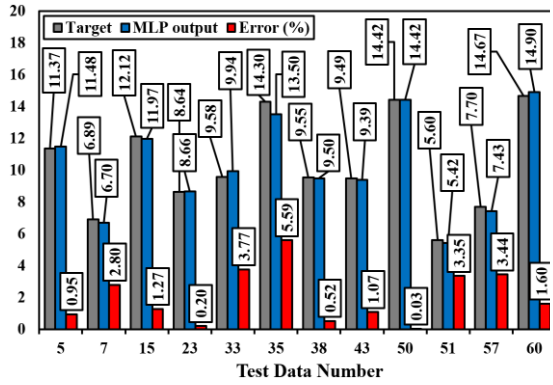

Fig. 7. Target values together with network outputs and absolute values of relative errors

Finally, the correlation between the predicted outputs by the MLP network and the targets obtained from the experiments has been illustrated in Fig. 8. The correlation coefficient between the test data set and predicted values is 99.54% for the best run.

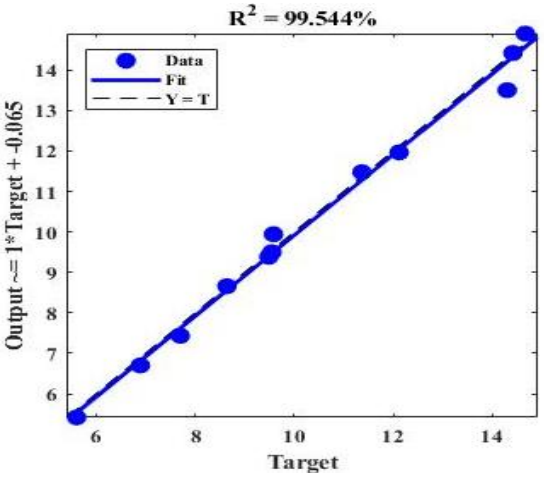

Fig. 8. Correlation plot between predicted values and targets obtained from the experiments (MLP network)

It should be noticed that according to the results presented in Table 2, since the standard deviation of errors, which is computed for 100 runs, is very low, it can be confidently said that the network performance remains acceptable in any further run. Overall, the results show that the MLP with a suitable construction can be a powerful tool for modeling the process, and additional analyses are now possible using the constructed model.

4.2. The RBF Model

As the new RBF in MATLAB software has been employed to construct the RBF neural network, the most critical parameters that should be carefully tuned are the spread (σ) and the maximum number of neurons (N). Here, the simulated annealing (SA) algorithm has been implemented to find the best combination of these parameters. In each iteration of the SA, an

RBF network is constructed using the two parameters mentioned. Then, a constructed network is run 30 times, and in each run, the test data set (containing 12 data) is picked up randomly from all data. The average value of relative error computed via Eq. (9) is considered as the objective that should be minimized. Therefore, the optimization problem is defined as:

$$\text{Min } f(\sigma.N) = AvgRE\ (\sigma.N)$$

$$0.01 \le \sigma \le 3, \quad 1 \le N \le 100$$

The initial temperature was considered to be about 22.19 degrees, which is 80 times higher than that obtained in the first iteration. If the initial temperature is chosen high enough, the algorithm can search maximum points of the search space. As the number of iterations increases, the temperature decreases using a linear relationship.

When the optimization process has finished, the optimum values of σ and N are presented and the best performance of the RBF network has been achieved. The SA convergence plot has been presented in Fig. 9.

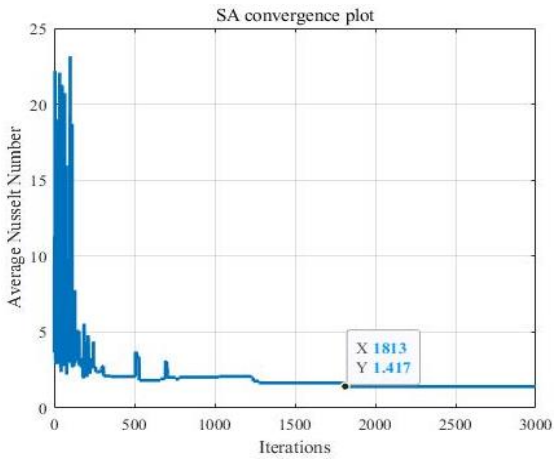

Fig. 9. The SA convergence procedure to improve the RBF performance

Fig. 8 displays that the network average error in the initial iterations is about 23%, but further iterations of the SA lead to improving the network performance. Therefore, the network error gradually decreases. It can be observed that after 1813 iterations, the lowest error value (1.417%) has been met. But, to ensure no further improvement occurs, the optimization procedure has continued up to 3000 iterations.

The predicted values against the targets for the train and test data sets are presented in Fig.s 10 and 11. In addition, the absolute values of relative errors computed via Eq. (8) for the optimal RBF network have been demonstrated in Fig. 12.

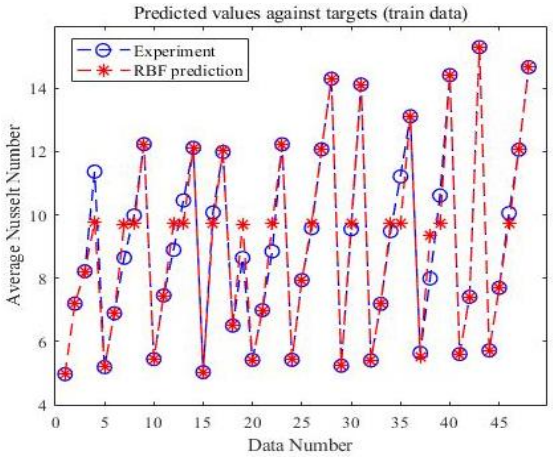

Fig. 10. The RBF performance based on the train data

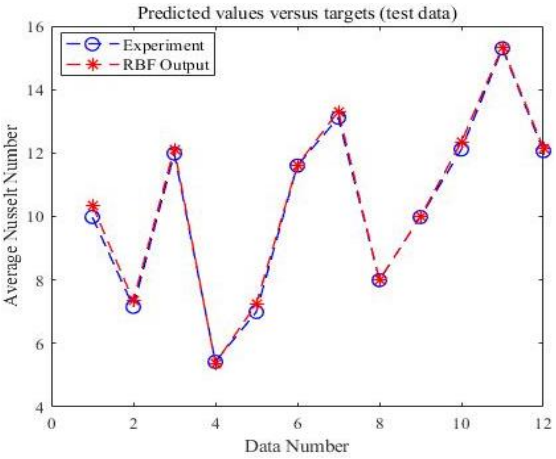

Fig. 11. The RBF performance based on the test data

The absolute values of relative errors computed via Eq. (8) for the optimal RBF network have been demonstrated in Fig. 12. The maximum error value is 3.74% according to data number 9, and the minimum one is 0.10% according to data number 53. Furthermore, 6 data have errors of less than 1%, and 9 data have relative errors of less than 2%. Moreover, the average relative error for the test data set is 1.42%, according to the optimization results.

Correlation between the predicted outputs by the optimal RBF network and the targets obtained from the experiments has been demonstrated in Fig. 13. The correlation coefficient between the test data set and predicted values is 99.91% for the optimized model. Fig.s 10-13 show that the network performance in predicting new data is acceptable. Now, further analyses of the process are possible using the constructed RBF model.

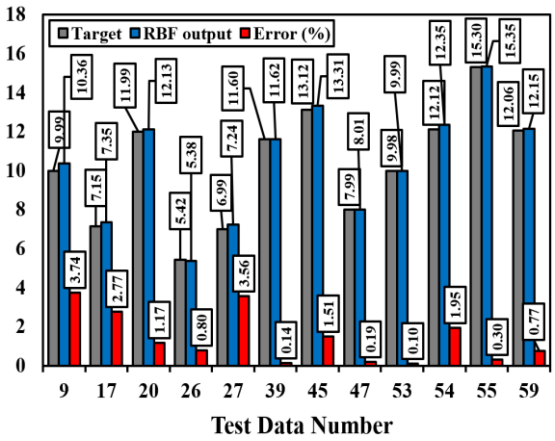

Fig. 12. Target values together with network outputs and absolute values of relative errors

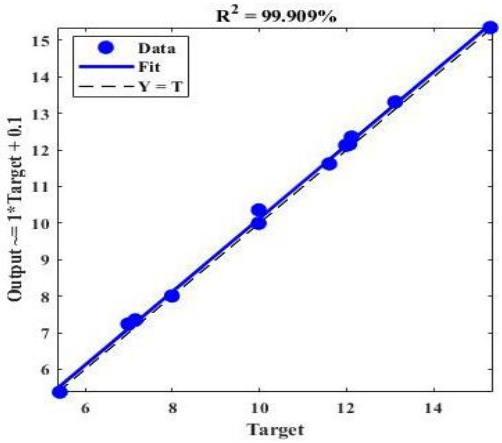

Fig. 13. Correlation plot between predicted values and targets obtained from the experiments (RBF network)

5. Conclusions

This study employed multi-layer perceptron (MLP) and radial basis function (RBF) neural networks to analyze the heat transfer process in a mini-channel heatsink with an alumina/water nanofluid. The optimal structure of the MLP was determined through trial and error, yielding the best network performance. On the other hand, the simulated annealing approach significantly increased the RBF network's performance.

Testing various structures of the MLP networks showed that inappropriately determining the number of hidden layers and hidden neurons could seriously damage the network performance. Furthermore, in the optimization process of RBF performance, it was seen that the inappropriate selection of the network parameters, highly affects the network error value so that in the initial iterations of the SA algorithm, the amount of network error can reach to more than 22%. The best combination of RBF parameters was found by increasing the iterations, and the errors fell below 1.5%. This clarifies the importance of the optimization process.

It can be concluded that the use of artificial neural networks can be used to simulate these processes effectively and efficiently, hence reducing the need for numerous laborious experimental procedures. In comparison, more data were predicted with an error of less than 2% when the optimized RBF network was used. Additionally, the RBF network has a stronger correlation coefficient between the projected data set and the targets than the MLP network, and the average relative error calculated using the RBF outputs is roughly 30% lower than the latter. The modeling time is a significant determining element when choosing the optimal technique. The RBF network optimization procedure took more than 60 minutes despite the fact that all MLP structures were run 100 times in less than 15 minutes (this run time might vary according to SA algorithm iterations and the number of RBF runs in each iteration). In summary, artificial neural networks are effective instruments for simulating these kinds of processes, and their application can help save a lot of time by avoiding a lot of laborious experimental procedures. Additionally, the RBF network performs more accurately while requiring less processing time than the MLP.

Nomenclature

A	Heat transfer area [m^2]
C_P	Specific Heat [J/(kg. K)]
c_k	Centre of the basis function associated with the kth node in the input space
$f(x)$	Objective function
$\bar{h}$	Average Heat Transfer Coefficient [W/(m. K)]
k	Thermal conductivity [W.(m. K)]
N	Number of channels
$\overline{Nu}$	Average Nusselt number
$\dot{Q}$	Heat transfer rate [W]
$q_{o,corr}$	Corrected electric power [W]
$q_{o,eff}$	Effective heat input absorbed by the working fluid [W]
q_o	Electric input power [W]
Re	Reynolds number
R^2	Correlation coefficient
T	Temperature in the SA algorithm [K]
w_k	Weight corresponding to the kth node of the hidden layer in RBFNN

Greeks and Symbols

ρ	Density [kg.m^{-3}]
φ_k	Processing function for the node number *k* of the hidden layer in RBFNN
ω	Concentration of nanoparticles [%]
σ	Spread

Subscription

in	Inlet
out	Outlet
w	Wall
corr	Corrected
h	Hydraulic

Abbreviation

ANN	Artificial Neural Network
MLP	Multi-Layer Perceptron
RBF	Radial Basis Function
SA	Simulated Annealing
CI	Computational Intelligence
FL	Fuzzy Logic
GAs	Genetic Algorithms
RBFNN	Radial Basis Transfer Function
MAPE	Mean Absolute Percentage Error
BP	Back Propagation
RE	Relative error
AvgRE	The average value of relative error
stdRE	Standard Deviation of the *AvgRE*
MinRE	Minimum value of relative error
CorrCoef	Correlation coefficient between the predicted outputs and their targets
RTDs	Resistance Temperature Detectors

Funding Statement

This research was funded by Ministry of Science and Technology (MOST110-2221-E006-146) in Taiwan.

Conflicts of Interest

The author declares that there is no conflict of interest regarding the publication of this article.

Data Availability

The data that support the findings of this study are available from the corresponding author upon reasonable request.

References

[1] Ho, C.J., Chen, W.C. and Yan, W.M., 2014. Correlations of heat transfer effectiveness in a minichannel heat sink with water-based suspensions of Al2O3 nanoparticles and/or MEPCM particles. *International Journal of Heat and Mass Transfer*, 69, pp.293-299.

[2] Hadi, F., Ali, H.M., Khattak, Z. and Janjua, M.M., 2024. An evaluation of heat transfer and pressure drop performance of superhydrophobic surfaced integral mini-channel heat sinks with nanofluids. *Journal of Thermal Analysis and Calorimetry*, pp.1-19.

[3] Ho, C.J., Hsieh, Y.J., Rashidi, S., Orooji, Y. and Yan, W.M., 2020. Thermal-hydraulic analysis for alumina/water nanofluid inside a mini-channel heat sink with latent heat cooling ceiling-An experimental study. *International Communications in Heat and Mass Transfer*, 112, p.104477.

[4] Ghasemi, S.E., Ranjbar, A.A., Hoseini, M.J. and Mohsenian, S., 2021. Design optimization and experimental investigation of CPU heat sink cooled by alumina-water nanofluid. *Journal of Materials Research and Technology*, 15, pp.2276-2286.

[5] Khan, M.Z.U., Younis, M.Y., Akram, N., Akbar, B., Rajput, U.A., Bhutta, R.A., Uddin, E., Jamil, M.A., Márquez, F.P.G. and Zahid, F.B., 2021. Investigation of heat transfer in wavy and dual wavy micro-channel heat sink using alumina nanoparticles. *Case Studies in Thermal Engineering*, 28, p.101515.

[6] Dastafkan, S.F., Azizi, Z., Mirzaei, M., Ghanavati, B. and Raei, B., 2024. Experimental study of the effect of alumina nanoparticles and channel waviness on the thermal performance of the nanofluid in a minichannel heat sink. *Journal of Thermal Analysis and Calorimetry*, 149(1), pp.505-518.

[7] Topcu, G., Ercetin, U. and Timuralp, C., 2023. CFD Analysis of Liquid-Cooled Heatsink Using Nanofluids in Computer Processors. *Scientia Iranica*.

[8] Saghafian, M., Seyedzadeh, H. and Moradmand, A., 2023. Numerical simulation of electroosmotic flow in a rectangular microchannel with use of magnetic and electric fields. *Scientia Iranica*.

[9] Hameed, S. and Saha, S., 2024. Hydro-thermal phenomena of oil-multi-walled carbon nanotubes nano-fluid flow through a rectangular channel: impact of obstacles. *Scientia Iranica*.

[10] Ramesh, K., Mebarek-Oudina, F., Ismail, A.I., Jaiswal, B.R., Warke, A.S., Lodhi, R.K. and Sharma, T., 2023. Computational analysis on radiative non-Newtonian Carreau nanofluid flow in a microchannel under the magnetic properties. *Scientia Iranica*, 30(2), pp.376-390.

[11] Saadoon, Z.H., Ali, F.H. and Sheikholeslami, M., 2023. Numerical investigation of heat transfer enhancement using (Fe3O4 and Ag-H2O) nanofluids in (converge-diverge) mini-channel heat sinks. Materials Today: Proceedings, 80, pp.2983-2996.

[12] Lan, Y., Feng, Z., Hu, Z., Zheng, S., Zhou, J., Zhang, Y., Huang, Z., Zhang, J. and Lu, W., 2023. Experimental investigation on the effects of swirling flow on flow boiling heat transfer and instability in a minichannel heat sink. *Applied Thermal Engineering*, 219, p.119512.

[13] Nemati, H., Moghimi, M.A. and Markides, C.N., 2023. Heat transfer characteristics of thermally and hydrodynamically developing flows in multi-layer mini-channel heat sinks. *International Journal of Heat and Mass Transfer*, 208, p.124052.

[14] Esfe, M.H., 2017. Designing a neural network for predicting the heat transfer and pressure drop characteristics of Ag/water nanofluids in a heat exchanger. *Applied Thermal Engineering*, 126, pp.559-565.

[15] Longo, G.A., Righetti, G., Zilio, C., Ortombina, L., Zigliotto, M. and Brown, J.S., 2020. Application of an Artificial Neural Network (ANN) for predicting low-GWP refrigerant condensation heat transfer inside herringbone-type Brazed Plate Heat Exchangers (BPHE). *International Journal of Heat and Mass Transfer*, 156, p.119824.

[16] Maddah, H., Ghazvini, M., Ahmadi, M.H., Bui, D.T. and Filho, E.P.B., 2021. Performance evaluation of a U-shaped heat exchanger containing hybrid Cu/CNTs nanofluids: experimental data and modeling using regression and artificial neural network. *Journal of Thermal Analysis and Calorimetry*, 143, pp.1503-1521.

[17] Moya-Rico, J.D., Molina, A.E., Belmonte, J.F., Tendero, J.C. and Almendros-Ibanez, J.A., 2019. Characterization of a triple concentric-tube heat exchanger with corrugated tubes using Artificial Neural Networks (ANN). *Applied Thermal Engineering*, 147, pp.1036-1046.

[18] Shojaeefard, M.H., Zare, J., Tabatabaei, A. and Mohammadbeigi, H., 2017. Evaluating different types of artificial neural network structures for performance prediction of compact heat exchanger. *Neural Computing and Applications*, 28, pp.3953-3965.

[19] Uysal, C. and Korkmaz, M.E., 2019. Estimation of entropy generation for Ag-MgO/water hybrid nanofluid flow through rectangular minichannel by using artificial neural network. *Politeknik Dergisi*, 22(1), pp.41-51.

[20] Tafarroj, M.M., Mahian, O., Kasaeian, A., Sakamatapan, K., Dalkilic, A.S. and Wongwises, S., 2017. Artificial neural network modeling of nanofluid flow in a microchannel heat sink using experimental data. *International Communications in Heat and Mass Transfer*, 86, pp.25-31.

[21] Motahar, S. and Jahangiri, M., 2020. Transient heat transfer analysis of a phase change material heat sink using experimental data and artificial neural network. *Applied thermal engineering*, 167, p.114817.

[22] Salehfekr Arabani, M.R., Pourmahmoud, N. and Mirzaii, I., 2021. Numerical and artificial neural network modeling study on the first-law and second-law performance of a novel helical heat sink filled with water–silver nanofluid. *Journal of Thermal Analysis and Calorimetry*, 145(4), pp.2225-2240.

[23] Zheng, X., Yang, R., Wang, Q., Yan, Y., Zhang, Y., Fu, J. and Liu, Z., 2022. Comparison of GRNN and RF algorithms for predicting heat transfer coefficient in heat exchange channels with bulges. *Applied Thermal Engineering*, 217, p.119263.

[24] Liu, Z. and Liu, J., 2022. Machine learning assisted analysis of an ammonia engine performance. *Journal of Energy Resources Technology*, 144(11), p.112307.

[25] Sun, M., Liu, Z. and Liu, J., 2023. Numerical investigation of the intercooler performance of aircraft piston engines under the influence of high altitude and cruise mode. *ASME Journal of Heat and Mass Transfer*, 145(6), p.062901.

[26] Yang, R., Liu, Z. and Liu, J., 2024. The methodology of decoupling fuel and thermal nitrogen oxides in multi-dimensional computational fluid dynamics combustion simulation of ammonia-hydrogen spark ignition engines. *International Journal of Hydrogen Energy*, 55, pp.300-318.

[27] Liu, J. and Liu, Z., 2024. In-cylinder thermochemical fuel reforming for high efficiency in ammonia spark-ignited engines through hydrogen generation from fuel-rich operations. *International Journal of Hydrogen Energy*, 54, pp.837-848.

[28] Ho, C.J., Chen, W.C., Yan, W.M. and Amani, M., 2017. Cooling performance of MEPCM suspensions for heat dissipation intensification in a minichannel heat sink. *International Journal of Heat and Mass Transfer*, 115, pp.43-49.

[29] Ho, C.J., Chen, W.C., Yan, W.M. and Amani, P., 2018. Contribution of hybrid Al2O3-water nanofluid and PCM suspension to augment thermal performance of coolant in a minichannel heat sink. *International Journal of Heat and Mass Transfer*, 122, pp.651-659.

[30] Ho, C.J., Chen, W.C. and Yan, W.M., 2014. Correlations of heat transfer effectiveness in a minichannel heat sink with water-based suspensions of Al2O3 nanoparticles and/or MEPCM particles. *International Journal of Heat and Mass Transfer*, 69, pp.293-299.

[31] Ho, C.J., Chen, W.C. and Yan, W.M., 2014. Experiment on thermal performance of water-based suspensions of Al2O3 nanoparticles and MEPCM particles in a minichannel heat sink. *International Journal of Heat and Mass Transfer*, 69, pp.276-284.

[32] Ho, C.J., Chen, W.C. and Yan, W.M., 2013. Experimental study on cooling performance of minichannel heat sink using water-based MEPCM particles. *International communications in heat and mass transfer*, 48, pp.67-72.

[33] Cheng, W.C., 2009. Heat Transfer Experiment on Forced Convection Performance of Water-Based Suspensions of Nanoparticles and/or MEPCM Particles in a Minichannel Heat Sink., *National Cheng-Kung University*.

[34] Ignatyev, D.I. and Khrabrov, A.N., 2015. Neural network modeling of unsteady aerodynamic characteristics at high angles of attack. *Aerospace Science and Technology*, 41, pp.106-115.

[35] Tafarroj, M.M. and Kolahan, F., 2019. Using an optimized RBF neural network to predict the out-of-plane welding distortions based on the 3-2-1 locating scheme. *Scientia Iranica*, 26(2), pp.869-878.

[36] Agrawal, S., Gobiha, D. and Sinha, N.K., 2019, January. Estimation of nonlinear airship parameters using modular neural network. In *2019 Fifth Indian Control Conference (ICC)* (pp. 45-50). IEEE.

[37] Tafarroj, M.M. and Kolahan, F., 2018. A comparative study on the performance of artificial neural networks and regression models in modeling the heat source model parameters in GTA welding. *Fusion Engineering and Design*, 131, pp.111-118.

[38] Tafarroj, M.M., Daneshazarian, R. and Kasaeian, A., 2019. CFD modeling and predicting the performance of direct absorption of nanofluids in trough collector. *Applied Thermal Engineering*, 148, pp.256-269.

[39] Kirkpatrick, S., Gelatt Jr, C.D. and Vecchi, M.P., 1983. Optimization by simulated annealing. *science*, 220(4598), pp.671-680.